

retinalysis-vascx: an explainable software toolbox for the extraction of retinal vascular biomarkers

Jose D. Vargas Quiros^{1,2}, Michael J. Beyeler^{5,6}, Sofia Ortín Vela^{5,6}, EyeNED Reading Center, VascX Consortium, Sven Bergmann^{5,6,7}, Caroline C.W. Klaver^{1,2,3,4} and Bart Liefers^{1,2}

¹Department of Ophthalmology, Erasmus University Medical Center, Rotterdam, the Netherlands

²Department of Epidemiology, Erasmus University Medical Center, Rotterdam, the Netherlands

³Department of Ophthalmology, Radboud University Medical Center, Nijmegen, the Netherlands

⁴Institute of Molecular and Clinical Ophthalmology, University of Basel, Switzerland

⁵Dept. of Computational Biology, University of Lausanne, Lausanne, Switzerland

⁶Swiss Institute of Bioinformatics, Lausanne, Switzerland

⁷Dept. of Integrative Biomedical Sciences, University of Cape Town, Cape Town, South Africa

ABSTRACT

Purpose: Automatic extraction of retinal vascular biomarkers from color fundus images (CFI) is crucial for large-scale studies of the retinal vasculature. We present VascX, an open-source Python toolbox specifically designed for automatic biomarker extraction from artery and vein segmentations obtained from CFIs.

Methods: Our approach starts from vessel segmentation masks; extracts their skeletons; builds undirected and directed vessel graphs; and resolves vessel segments into longer vessels. A comprehensive set of biomarkers is derived, including vascular density, bifurcation angles, central retinal equivalents (CREs), tortuosity, temporal angles, and image quality metrics. Spatially localized biomarkers are calculated over grids placed relative to the fovea and optic disc.

Results: VascX is made open-source and released via GitHub and PyPI. Documentation and examples are provided to demonstrate its functionality and support reproducible vascular analyses. Biomarker visualizations can be generated on any input image, facilitating explainability. A key feature of VascX is its region awareness; using the fovea, optic disc and CFI bounds as anatomical landmarks to detect when a specific biomarker is not computable.

Conclusions: VascX provides a reliable, explainable, and easily modifiable feature-extraction toolbox that complements high-fidelity segmentation to produce spatially standardized retinal vascular biomarkers. Our graph-based biomarker computation stages support reproducible, region-aware measurements suited for large-scale clinical and epidemiological research.

Translational Relevance: VascX advances oculomics by enabling easy extraction of existing biomarkers and rapid experimentation with new biomarkers. Its robustness and computational efficiency facilitates scalable deployment in large databases. Open-source distribution via PyPI lowers barriers to adoption for ophthalmic researchers and clinicians.

Introduction

Artificial intelligence (AI) has rapidly changed ophthalmic research by enabling the quantitative, automated analysis of imaging at scale. Modern deep learning (DL) applied to color fundus imaging (CFI) has demonstrated the ability to automatically detect ophthalmic disease. In recent years the field of oculomics has taken this a step further by utilizing the eye to understand systemic health¹⁻³. Non-invasive CFI allows for time and cost-efficient examination of the arteriolar and venular retinal vasculature, also opening the door for large-scale analysis of the vasculature in existing population-based cohorts and clinical databases. Today, substantial evidence links key retinal vascular features to hypertension, kidney disease, stroke subtypes, and overall cardiovascular risk².

Relevant retinal vascular biomarkers include the central retinal arteriolar / venular equivalents (CRAE/CRVE), artery-vein ratio (AVR), bifurcation angles, tortuosity/fractal dimension and bifurcation counts. These features capture changes in the vasculature due to hypertension, hemodynamic status, and network remodeling/efficiency, and have each been linked to target organ damage and incident vascular events^{2,4}.

Prior work on the technical challenge of automatically extracting biomarkers from CFIs has laid a strong foundation. PVBM provides a modular Python toolbox for computing a diverse set of vascular biomarkers from pre-segmented vessel maps, including branching angles, endpoints and intersections⁵. AutoMorph delivers a comprehensive end-to-end DL pipeline that includes standardized morphological measurements like caliber, tortuosity, and measures of vascular complexity⁶. Together, these tools have made vascular analysis on fundus image more accessible.

Nevertheless, important technical gaps remain. Most notably PVBM and AutoMorph do not use the location of the fovea for feature computation, preventing the extraction of more localized biomarkers computed over regions or grids defined relative to the optic-disc-fovea axis. The topological data representation in both tools is limited to an undirected graph, preventing the extraction of topological features that rely on the directedness of the vessel tree graph. Furthermore, both tools lack utilities for easily visualizing the computed features, which limits interpretability.

VascX addresses these needs with a graph-based feature extraction toolbox that utilizes AI disc segmentations and fovea locations for localized feature extraction⁷. The pipeline transforms image-level vessel masks into four different representations sequentially: skeletons, undirected graphs, directed trees with the optic disc as the root, and resolved vessel trees. Biomarkers are then computed from the most appropriate representation stage (e.g., mask-based density, node-based bifurcation counts/angles, segment-based diameter/length/tortuosity, and OD-fovea-aligned spatial features such as CRE and temporal arcade angles). Critically, VascX computes local features using grids and regions defined relative to the fovea and optic disc landmarks, facilitating harmonized reporting and region-specific analyses relevant to clinical translation. The VascX pipeline has

already been applied in a multi-cohort study on the phenotypic and genetic characteristics of retinal vascular parameters and their association with diseases⁴.

In this paper, we present a transparent, well-documented, and easily modifiable Python toolbox designed to accelerate methodological innovation and large-scale, reproducible oculomics research. Our contributions are the following:

- We provide an easy-to-use toolbox for analyzing the retinal vasculature. Our toolbox can compute a comprehensive catalog of morphology, topology, caliber, and spatially localized biomarkers, including OD–fovea–aligned and ETDRS-style grid features, from artery–vein–resolved segmentations.
- We present results on the reproducibility of VascX biomarkers across images of the same eye.
- VascX enables rapid experimentation with improved retinal biomarkers via a clear, modular graph-based pipeline and well-documented APIs.
- The toolbox is open source and easily accessible in Python via PyPI.

Methods

Our package was developed entirely in Python using standard data science and image manipulation packages: numpy, opencv, Pillow, scikit-learn, skimage. The package has only open-source dependencies. In this work, we present a first public version of the package. We will follow semantic versioning for future versions.

The VascX feature extraction pipeline operates on image segmentations (usually generated by AI models) and outputs a CSV file with features or biomarkers computed from them. The previous step of model segmentation has been addressed in previous work^{6–8}. VascX operates on image files individually or in bulk. It accepts all input image formats readable by Pillow.

Software Summary

VascX is available at:

<https://github.com/Eyened/retinalysis-vascx>

under an open-source license (GNU Affero General Public License v3.0). The package is also available in the Python package index (PyPI) under the name retinalysis-vascx.

Usage

Installation of the VascX feature extraction pipeline amounts to creating a virtual environment and installing the pipeline as a Python package:

```
pip install retinalysis-vascx
```

We provide helpers and instructions for running in batches. The entire pipeline can be ran in two stages:

1. Segmentation. To extract all the necessary segmentations from the images:

```
vascx run-models /path/to/cfis /path/to/segmentations
```

This command will store model outputs and some intermediate files in a folder structure with matching filenames:

```
/path/to/segmentations
- preprocessed_rgb/ - preprocessed fundus images
- artery_vein/ - artery-vein model segmentations
- vessels/ - vessel model segmentations
- disc/ - optic disc model segmentations
- bounds.csv - contains the bounds of the fundus image
- fovea.csv - model predictions of the fovea locations for each image
- quality.csv - model estimations of CFI quality
```

This command makes use of previously published segmentation, regression and keypoint localization AI models⁷ to segment vessels, arteries, veins and disc, obtain fovea locations and estimate image quality. The folders (preprocessed_rgb/, artery_vein/, vessels/, disc/) contain matching filenames (one per input image). The CSV files contain one row per input image.

2. Biomarker extraction. The second stage operates on the output from the first stage:

```
vascx calc-biomarkers /path/to/segmentations /path/to/features.csv --feature_set full --n-jobs 8 --logfile /path/to/logfile.txt
```

The biomarkers are stored to /path/to/features.csv.

Vascular biomarker computation

VascX processes the input artery-vein model segmentations into separate artery and vein masks. These are then separately processed through four main stages of computation, each producing different data representations:

- **Input masks:** np.ndarray[bool] per layer; optic disc and fovea metadata from segmentation models.
- **Stage 1 - Skeleton:** We first hole-fill the predicted binary vessel map to obtain a clean binary mask; when an optic disc mask is available, the disc region is excluded to prevent spurious centerlines. The skeleton is computed with skimage skeletonization on binary, yielding single-pixel-wide centerlines that preserve network topology. This pixel-level representation underpins coverage and diameter sampling and serves as the substrate for graph construction.

- **Stage 2 - Undirected graph:** From the skeleton we build a NetworkX Graph whose nodes correspond to end/junction points and whose edges follow the chain of centerline pixels between them. Each edge carries a Segment that stores the ordered centerline, arclength and geometric summaries; splines are fitted on demand to the centerline to enable robust diameter and angle estimation. This representation supports segment-level filtering and aggregation without yet imposing flow direction.
- **Stage 3 - Directed digraph:** We orient the undirected graph into a DiGraph by rooting each connected component at the optic disc and directing edges away from the disc. Roots are identified as the end-node per component closest to the disc center. Vessel segments are directed edges carrying geometry and derived properties (length, median diameter, curvature). The directed graph representation is an intermediate step in the identification of bifurcations. A distance-transform-based assignment maps each pixel in the binary vessel mask (stage 1) to its nearest segment.
- **Stage 4 - Resolved vessels:** In previous stages vessel segments are defined only between nodes in the skeleton / graph representation. This means that the presence of even a small vascular branch on a large vessels will cause it to be split into two segments. To facilitate the computation of biomarkers on longer, potentially more anatomically relevant vessel trajectories we run a recursive vessel-resolution algorithm on the DiGraph. For each root, an aggregated caliber is propagated along outgoing paths using a length-weighted running statistic of per-edge median diameters. At every bifurcation, the branch with the largest aggregated caliber is taken as the principal continuation; non-selected branches are closed and emitted as resolved segments. Consecutive edges along a resolved path are concatenated into a single Segment by merging centerlines (and attached pixels), yielding a simplified directed graph whose resolved_segments approximate individual vessels between major bifurcations. This reduces fragmentation from skeletonization while preserving topology for trajectory-level tortuosity and OD-fovea-aligned measures.

Finally, biomarkers are extracted from one or a combination of these data representations. Mask-based biomarkers such as vascular density, for example, are calculated on the input masks, while topological features such as bifurcation angles use the directed graph and nodes extracted in stage 4. Figure 1 exemplifies the different stages of computation for a sample set of CFIs.

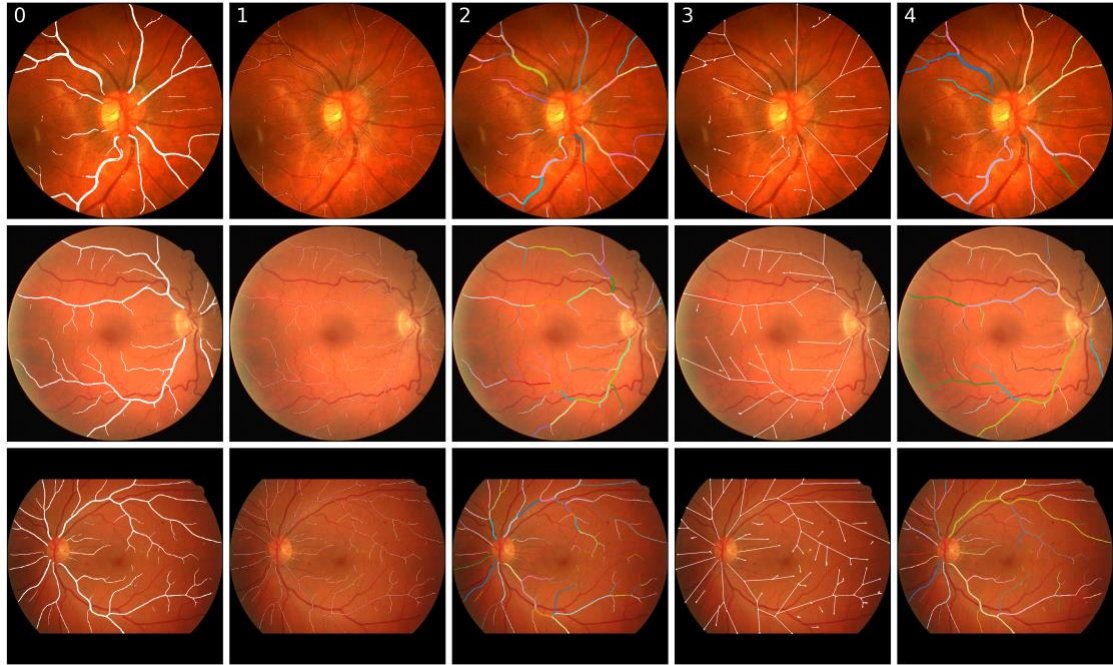


Figure 1. From left to right, stages of computation in the VascX pipeline for three sample CFIs: 0) input binary mask for the arteries, 1) skeletonization or centerline computation, 2) vessel segments are extracted from the skeleton, and mapped back to their centerline and mask, 3) a directed graph consisting of multiple trees with the optic disc as root, 4) segments are resolved into potentially more anatomically meaningful structures for biomarker measurements.

Biomarkers

VascX computes retinal vascular biomarkers from standardized representations (binary masks, undirected/directed graphs, resolved vessels). Below we describe each feature with the exact quantity being estimated and the equations used. Throughout, B denotes the stage-1 binary vessel mask, S the set of eligible directed segments with lengths ($_i$), and R an analysis region of interest; cardinalities count pixels, and distances are in pixels unless noted.

VascularDensity. The fraction of retinal area occupied by vessels in R , computed on the binary mask B :

$$D = \frac{|B \cap R|}{|R|}.$$

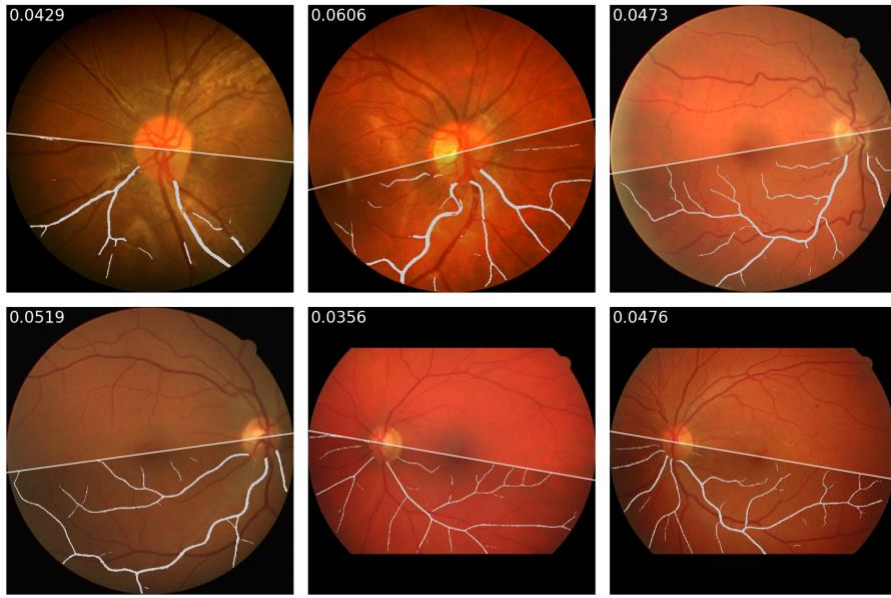


Figure 2. Examples of vascular density computation on the lower hemifield. The computed value is show on the top left corner of each sample.

BifurcationCount. The count of branching points in the directed graph (stage-3). Let \mathcal{B} be the set of bifurcation nodes with positions p_b :

$$C = \sum_{b \in \mathcal{B}} \mathbf{1} [p_b \in R].$$

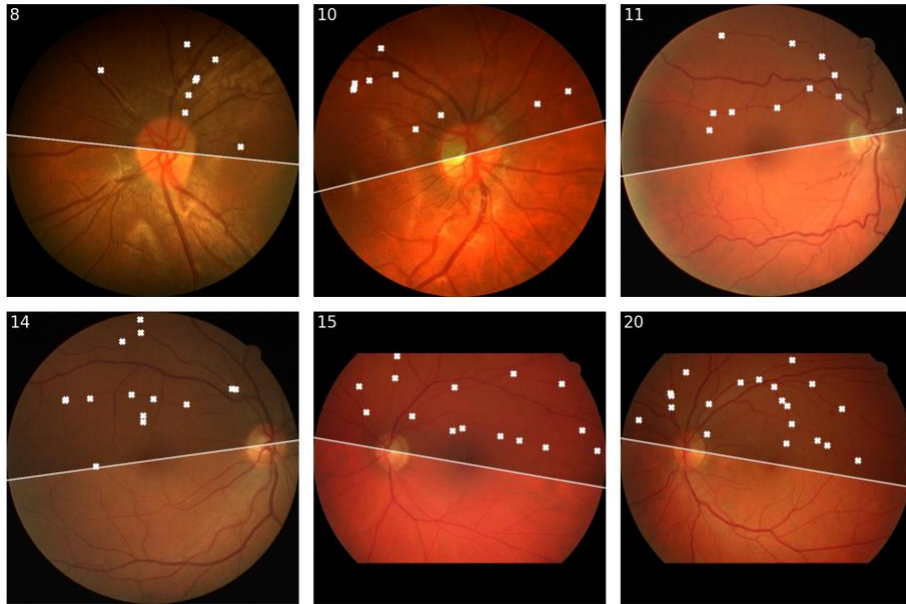


Figure 3. Examples of bifurcation counts computation on the superior hemifield. The computed value is show on the top left corner of each sample.

BifurcationAngles. For each bifurcation b at position p_b , outgoing branch directions are estimated by sampling the branches' splines at distance δ from the node along each branch at points q_1 and q_2 . Unit vectors (u_b, v_b) are defined from the bifurcation point to the sample points:

$$u_b = \frac{q_1 - p_b}{\| q_1 - p_b \|}, \quad v_b = \frac{q_2 - p_b}{\| q_2 - p_b \|},$$

and the bifurcation angle is defined as the angle between these vectors:

$$\theta_b = \arccos(u_b \cdot v_b), \quad \theta_b \in [0^\circ, 180^\circ].$$

Angles exceeding 160° are discarded as non-bifurcating continuations. Summary statistics (e.g., mean/median) are reported across valid nodes.

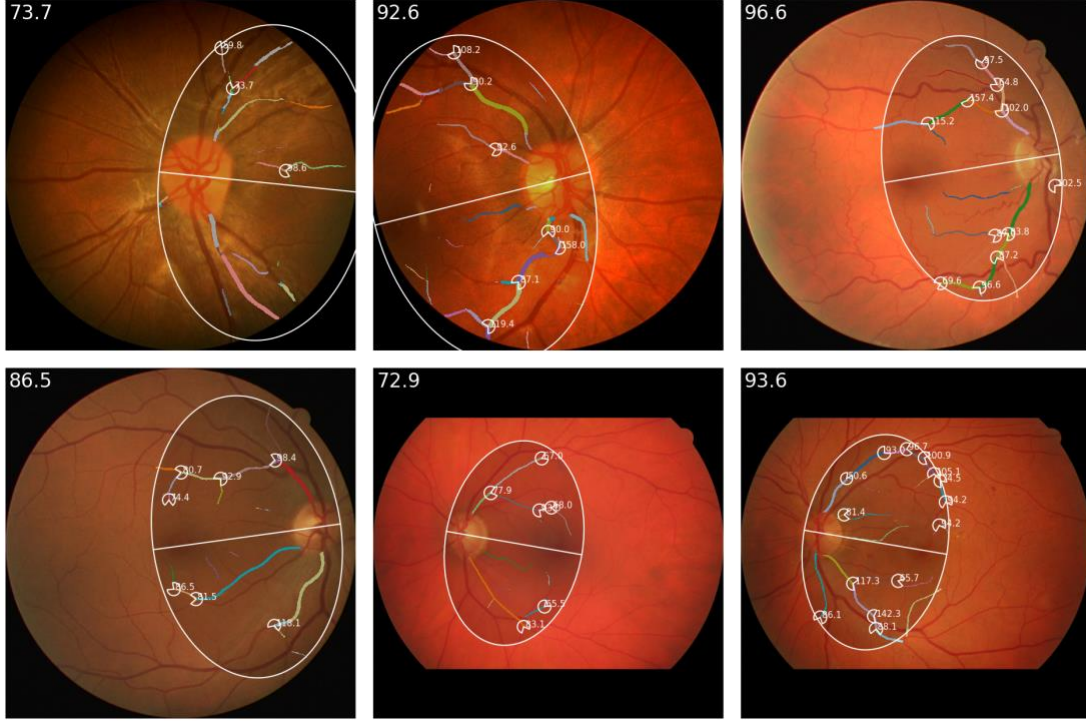


Figure 4. Examples of bifurcation angle computation on an elliptical region located between the fovea and optic disc. This region is consistently visible in optic disc and macula-centered images. The computed value is show on the top left corner of each sample.

Caliber. For each segment i , diameters are sampled along a spline fitted to its skeleton by projecting spline normals to the vessel boundary on B . The per-segment diameter is the median along its arclength. The reported caliber aggregates over eligible segments (length $\ell_i \geq \ell_{\min}$):

$$\text{Caliber} = g(\{d_i : i \in S\}),$$

where (g) is a robust statistic (typically the median).

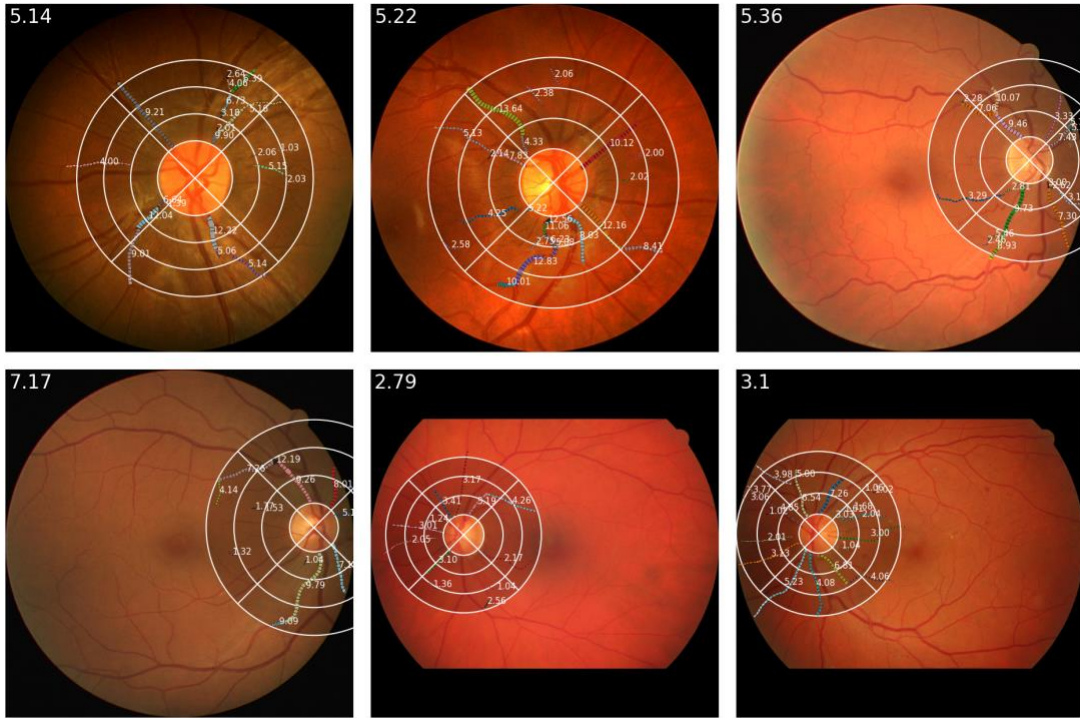


Figure 5. Examples of caliber computation over a region defined around the optic disc. The computed value is show on the top left corner of each sample.

Tortuosity. Three complementary measures are provided per segment (or per resolved vessel). Let $L_{\text{arc},i}$ be arclength and $L_{\text{chord},i}$ the end-to-end Euclidean distance.

- Distance factor:

$$T_i^{\text{DF}} = \frac{L_{\text{arc},i}}{L_{\text{chord},i}}.$$

- Curvature-based measure, using planar curvature $\kappa_i(s)$ and OD–fovea distance d_{ODF} for scale normalization:

$$T_i^{\kappa} = \frac{1}{L_{\text{arc},i}} \int_0^{L_{\text{arc},i}} |\kappa_i(s)| ds \cdot d_{ODF}.$$

- Inflection count (number of curvature sign changes along the centerline):

$$T_i^{\text{INF}} = N_{\text{inflections}}^{(i)}.$$

When reporting a single score over multiple segments, length-weighted aggregation may be used for normalization:

$$T_{\text{tot}} = \sum_{i \in S} \left(\frac{\ell_i}{\sum_{j \in S} \ell_j} \right) t_i,$$

with t_i any of the measures above.

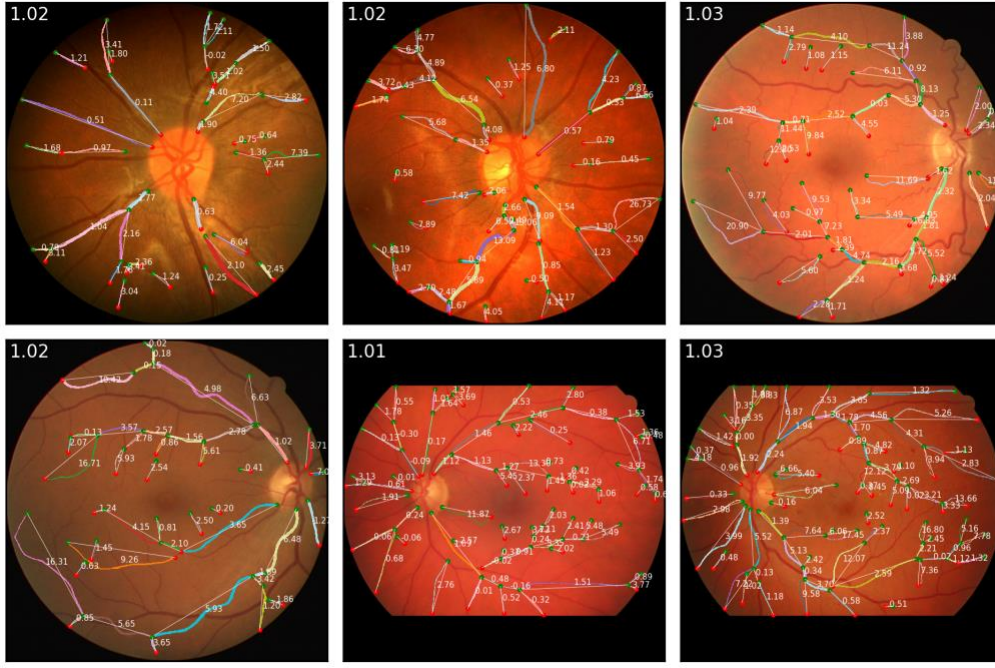


Figure 6. Examples of tortuosity computation over the entire visible region. The computed value is shown on the top left corner of each sample.

CRE (Central Retinal Equivalents). Concentric circles centered at the optic disc are intersected with the vessel network. At each radius r , up to M crossings with the largest segment median diameters are retained and recursively reduced via the Hubbard rule with a constant c (arteries: 0.88; veins: 0.95):

$$d \leftarrow c \sqrt{d_1^2 + d_2^2}$$

applied pairwise until a single equivalent caliber d_r remains. The final CRE is the median of $\{d_r\}$ across radii.

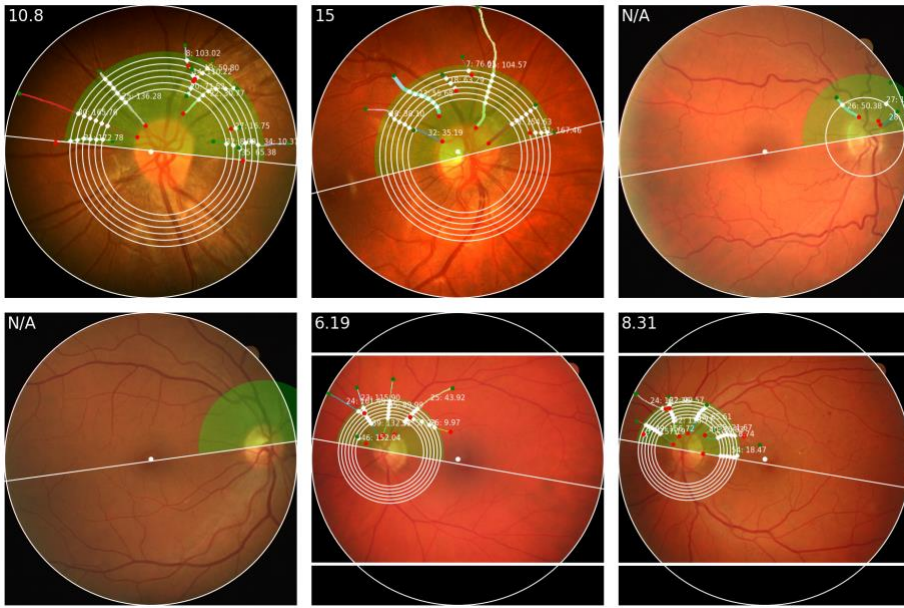


Figure 7. Examples of central retinal equivalent (CRE) computation on the superior hemifield. The computed value is show on the top left corner of each sample.

TemporalAngle. On each concentric circle of radius (r), the two dominant temporal vessels are identified by diameter and spatial continuity. The angle at the disc center is

$$\theta_r = \angle(\overrightarrow{OD p_1(r)}, \overrightarrow{OD p_2(r)}),$$

and the reported value is the median over radii.

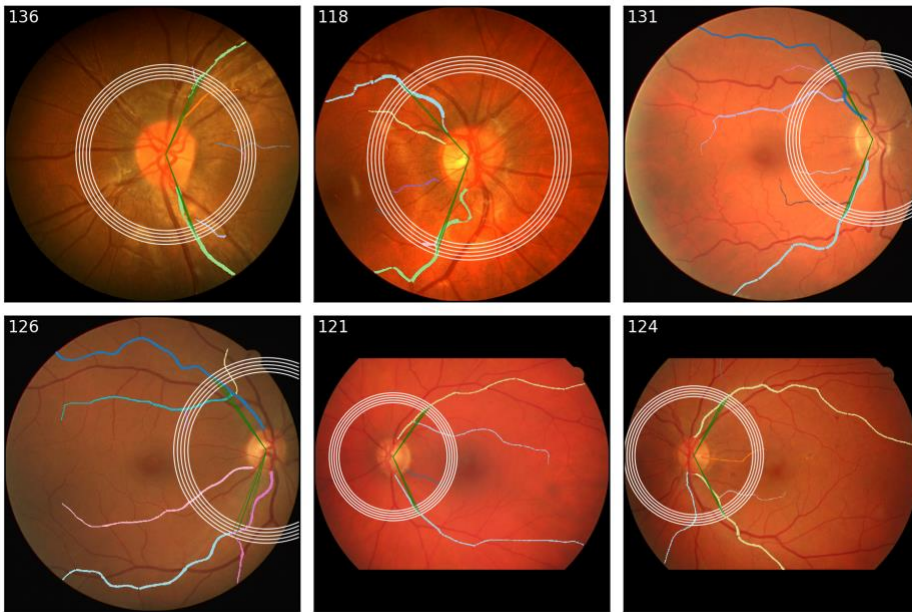


Figure 8. Examples of temporal angle computation capturing the opening angle of the main vascular arcades. The computed value is show on the top left corner of each sample.

Sparsity. Let $\text{DT}(x)$ represent the distance transform over R , ie. the normalized Euclidean distance to the nearest vessel pixel (scaled by d_{ODF}). Over pixels in R we report either the mean or the largest local maximum:

$$S_{\text{mean}} = \frac{1}{|R|} \sum_{x \in R} \text{DT}(x), \quad S_{\text{max}} = \max_{x \in R \cap \text{local maxima}} \text{DT}(x).$$

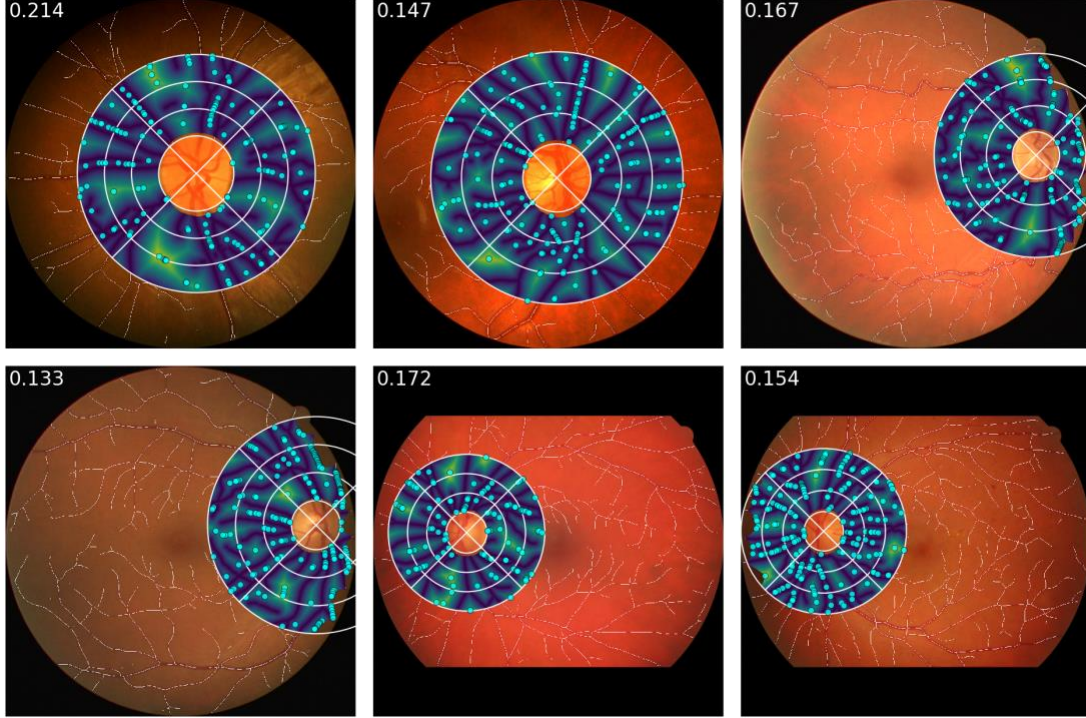


Figure 9. Examples of sparsity computation over a grid defined around the optic disc. The computed value is shown on the top left corner of each sample.

VarianceOfLaplacian. For the fundus image I (grayscale), compute the discrete Laplacian $L = \Delta I$. Image sharpness is summarized as the variance over R :

$$\text{Var}\{L(x): x \in R\}.$$

DiscFoveaDistance. With optic disc center c_{OD} and fovea position p_f ,

$$d_{ODF} = \|c_{OD} - p_f\|_2.$$

Feature localisation

Most features in VascX accept an optional `grid_field` parameter that specifies the region of interest. A grid can be understood as a subdivision of the image space (eg. the ETDRS grid), and a grid field as a particular region within that subdivision (eg. the outer ring of the ETDRS grid, the superior hemifield, or the entire grid). The optic disc mask and fovea

position (e.g., OD–fovea axis) are usually used to orient geometry. Several grids are included with VascX (e.g., ETDRS grid, disc-centered grid, superior and inferior hemifields).

Given a field, features include only the structures that lie within it, using heuristics appropriate to the object being measured: - Segments and full vessels: included when a sufficient fraction of their centerline lies inside the field (using a default coverage threshold). - Nodes (endpoints, bifurcations): included if their coordinates fall inside the field. - Pixel/area-based measures (e.g., vascular density, tortuosity maps): computed from the pixels inside the field mask only. - Structures outside the chosen field are ignored for aggregation and summarization.

For a chosen field, the platform evaluates the fraction within the bounds of the CFI. If the fraction within bounds is too small (typically < 0.5), biomarker computation may return a null value to indicate an invalid measurement.

VascX includes the following predefined grids: - **EllipseGrid**: ellipse centered midway between disc and fovea, major axis along OD–fovea. This grid has consistently high visibility in both optic disc and macula centered images. Fields: FullGrid, Superior, Inferior. - **CircleGrid**: circle centered midway between disc and fovea (radius derived from OD–fovea distance and disc size). This grid provides consistent measurements on macula-centered images. Fields: FullGrid, Superior, Inferior. - **ETDRSGrid**: classic macula-centered ETDRS layout with rings (Center, Inner, Outer), quadrants (Superior, Inferior, Nasal, Temporal, plus Left/Right), and subfields (CSF, SIM, NIM, TIM, IIM, SOM, NOM, TOM, IOM). - **DiscCenteredGrid**: disc-anchored rings (inner, center, outer) and quadrants (superior, inferior, nasal, temporal, plus left/right), taking laterality into account. This grid is meant for consistent measurements on disc-centered images. - **HemifieldGrid**: superior/inferior half-planes split relative to the OD–fovea axis. Fields: FullGrid, Superior, Inferior.

Potential uses for the software

The VascX pipeline has a variety of potential use cases:

- **Oculomics and cardiovascular risk modeling**: Generate standardized, OD–fovea-aligned and ETDRS-grid biomarkers (morphology, topology, caliber) from artery–vein–resolved segmentations to support association studies and risk prediction for systemic outcomes.
- **Clinical and epidemiological research**: Report region-aware measurements (e.g., CRE, temporal arcade angle, tortuosity) in harmonized subfields, enabling reproducible, cross-center analyses and longitudinal studies, including reproducibility across repeat images of the same eye.
- **Population-scale pipelines and biobanks**: Run high-throughput batch extraction from pre-segmented images to produce analysis-ready feature tables suitable for large cohorts and multi-center datasets.

- **Biomarker development and benchmarking:** Use the modular, graph-based pipeline (skeleton → undirected graph → directed tree → resolved vessels) to prototype and compare new biomarkers or aggregation strategies with clear intermediate representations.
- **Adaptation to other modalities or use cases:** The VascX pipeline is highly modular and its building blocks may be adapted to different modalities or extended with new functionality.

Limitations of the software

VascX relies on external segmentations (vessels, artery/vein, optic disc, fovea), and their accuracy directly conditions all derived biomarkers. Errors such as missed or spurious vessels, artery–vein misclassification, or mislocalized disc/fovea—often caused by fundus image quality issues (e.g., blur, artifacts, illumination, limited field-of-view)—can bias both global and region-aware (ETDRS, OD–fovea–aligned) measurements. Users should treat segmentation quality and image quality as potential confounders and assess whether these preconditions are adequate for their study; sensitivity analyses and additional QC may be warranted before deciding to use the software in a given setting. The authors encourage and welcome follow-up work to quantify and mitigate the effects of image quality and segmentation errors on retinal vascular biomarkers.

A second limitation of the pipeline is that it is currently designed specifically for enface images, usually containing either the fovea or optic disc. However, its modular design and clear structure enables its adaptation to other use cases, potentially including the analysis of 3D volumes.

Acknowledgments

The authors acknowledge the staff of the Eyened Reading Center for their different roles in the project. Special acknowledgement to the Sinergia consortium for conceiving and supporting this project; and for their valuable feedback on the VascX platform. This work was funded by the Swiss National Science Foundation grant no. CRSII5 209510. Generative AI was used in the preparation of this manuscript as assistance in writing and proofreading. Google Gemini 2 and 3 were used in the period between July 1, 2025 and January 26, 2026.

References

1. Patterson, E. J. *et al.* Oculomics: A Crusade Against the Four Horsemen of Chronic Disease. *Ophthalmol Ther* **13**, 1427–1451 (2024).
2. Zhu, Z. *et al.* Oculomics: Current concepts and evidence. *Prog Retin Eye Res* **106**, 101350 (2025).
3. Wagner, S. K. *et al.* Insights into Systemic Disease through Retinal Imaging-Based Oculomics. *Transl Vis Sci Technol* **9**, 6 (2020).
4. Ortín Vela, S. *et al.* Phenotypic and Genetic Characteristics of Retinal Vascular Parameters and their Association with Diseases. *medRxiv* <https://doi.org/10.1101/2023.07.07.23292368> (2023) doi:10.1101/2023.07.07.23292368.
5. Fhima, J. *et al.* PVBM: A Python Vasculature Biomarker Toolbox Based on Retinal Blood Vessel Segmentation. in *Computer Vision – ECCV 2022 Workshops* (eds Karlinsky, L., Michaeli, T. & Nishino, K.) 296–312 (Springer Nature Switzerland, Cham, 2023). doi:10.1007/978-3-031-25066-8_15.
6. Zhou, Y. *et al.* AutoMorph: Automated Retinal Vascular Morphology Quantification Via a Deep Learning Pipeline. *Translational Vision Science & Technology* **11**, 12 (2022).
7. Vargas Quiros, J., Liefers, B., van Garderen, K. A., Vermeulen, J. P. & Klaver, C. VascX Models: Deep Ensembles for Retinal Vascular Analysis From Color Fundus Images. *Trans. Vis. Sci. Tech.* **14**, 19 (2025).
8. Fhima, J., Van Eijgen, J., Billen Moulin-Romsée, M. I., & others. LUNet: deep learning for the segmentation of arterioles and venules in high resolution fundus images. *Physiological Measurement* **45**, 10.1088/1361-6579/ad3d28 (2024).

Author information

VascX Consortium:

Ciara Bergin 3; Sven Bergmann 1,2,4; Michael Beyeler 1,2,5; Dennis Bontempi 1,2; Sacha Bors 1,2; Leah Böttger 1,2; Bogdan Draganski 5,6,7; Adham Elwakil 3,8; Györgyi V. Hamvas 9,10; Janna Hastings 11,12; Ilaria Iuliani 1,2; Caroline C.W. Klaver 13,14,15,16; Ihor Kuras 6,7; Bart Liefers 13,14; Ilenia Meloni 3,8; Sofia Ortin Vela 1,2; David Presby 1,2; Ian Quintas 1,2; José Vargas Quiros 13,14,; Marc Schindewolf 9,10; Reinier O. Schlingemann 3,17; Mattia Tomasoni 3,8; Olga Trofimova 1,2.

1 *Department of Computational Biology, University of Lausanne, Lausanne, Switzerland*

2 *Swiss Institute of Bioinformatics, Lausanne, Switzerland*

3 *Department of Ophthalmology, University of Lausanne, Fondation Asile des Aveugles, Jules Gonin Eye Hospital, Lausanne, Switzerland.*

4 *Department of Integrative Biomedical Sciences, University of Cape Town, Cape Town, South Africa*

5 *Insel University Hospital Bern, Switzerland*

6 *Department of Neurology, Max Planck Institute for Human Cognitive and Brain Sciences, Germany*

7 *Department of Clinical Neuroscience, Lausanne University Hospital and University of Lausanne, Switzerland*

8 *Platform for Research in Ocular Imaging, Fondation Asile des Aveugles, Jules Gonin Eye Hospital, Lausanne, Switzerland.*

9 *Inselspital, Bern University Hospital, University of Bern, Switzerland.*

10 *Department for BioMedical Research, Bern University Hospital, University of Bern, Switzerland.*

11 *Institute for Implementation Science in Health Care, Faculty of Medicine, University of Zurich, Zürich, Switzerland*

12 *School of Medicine, University of St Gallen, St. Gallen, Switzerland*

13 *Department of Ophthalmology, Erasmus University Medical Center, Rotterdam, The Netherlands.*

14 *Department of Epidemiology, Erasmus University Medical Center, Rotterdam, The Netherlands.*

15 *Department of Ophthalmology, Radboud University Medical Center, Nijmegen, the Netherlands.*

16 *Institute of Molecular and Clinical Ophthalmology, University of Basel, Switzerland.*

17 *University Medical Centres, Amsterdam, The Netherlands.*